Cumulative latency advance underlies fast visual processing in desynchronized brain state

Xu-dong Wang[a,1], Cheng Chen[a,b,1], Dinghong Zhang[a,b], and Haishan Yao[a,2]

[a]Institute of Neuroscience and State Key Laboratory of Neuroscience, Shanghai Institutes for Biological Sciences, Chinese Academy of Sciences, and [b]Graduate University of Chinese Academy of Sciences, Shanghai 200031, China

Edited* by Mu-ming Poo, University of California, Berkeley, CA, and approved November 25, 2013 (received for review August 27, 2013)

Fast sensory processing is vital for the animal to efficiently respond to the changing environment. This is usually achieved when the animal is vigilant, as reflected by cortical desynchronization. However, the neural substrate for such fast processing remains unclear. Here, we report that neurons in rat primary visual cortex (V1) exhibited shorter response latency in the desynchronized state than in the synchronized state. In vivo whole-cell recording from the same V1 neurons undergoing the two states showed that both the resting and visually evoked conductances were higher in the desynchronized state. Such conductance increases of single V1 neurons shorten the response latency by elevating the membrane potential closer to the firing threshold and reducing the membrane time constant, but the effects only account for a small fraction of the observed latency advance. Simultaneous recordings in lateral geniculate nucleus (LGN) and V1 revealed that LGN neurons also exhibited latency advance, with a degree smaller than that of V1 neurons. Furthermore, latency advance in V1 increased across successive cortical layers. Thus, latency advance accumulates along various stages of the visual pathway, likely due to a global increase of membrane conductance in the desynchronized state. This cumulative effect may lead to a dramatic shortening of response latency for neurons in higher visual cortex and play a critical role in fast processing for vigilant animals.

state-dependent temporal processing | synaptic inputs | hierarchical accumulation

Fast reaction is essential for the survival of animals, such as when detecting and fleeing a predator. Humans or animals react rapidly in a vigilant state (1–3). The vigilance level of animals (also humans) varies with brain state, which can be characterized by the patterns of population activities measured by electroencephalogram (EEG) and local field potential (LFP) (4, 5). Although brain state exhibits diverse activity patterns, it can be broadly classified into a desynchronized state dominated by small-amplitude, high-frequency activities, and a synchronized state dominated by large-amplitude, low-frequency fluctuations (4, 5). The brain operates in the desynchronized state when the animal is alert or vigilant, whereas it operates in the synchronized state when the animal is quiescent or drowsy (4, 5). To understand the neural substrate for fast processing in the vigilant state, it is important to compare response latencies in the two brain states for sensory cortical neurons, which are at the initial stage along the sensorimotor pathway.

Brain state has a dominant impact on both resting properties (6, 7) and sensory evoked responses (4, 8, 9) of cortical neurons. For the visual system, although brain state or behavioral state can modulate response amplitude, spatial receptive field, and temporal frequency tuning of the neurons in the early visual pathway (10–13), it is not clear whether brain state can modulate response latency of primary visual cortex (V1) neurons. Furthermore, the cellular and network mechanisms for brain state modulation of visual response remain largely unknown. It is suggested that background synaptic bombardments regulate membrane potential and input conductance of cortical neurons, and thus significantly influence the temporal properties of synaptic integration by the neurons (14, 15). In this study, we raised and tested a hypothesis that brain state can modulate response latency of V1 neurons by changing background synaptic inputs.

We found in this study that the response latency of V1 neurons was shorter in the desynchronized state than in the synchronized state, in both awake and anesthetized rats. In vivo whole-cell recording from the same V1 neurons undergoing the two states showed that both the resting and visually evoked conductances were higher in the desynchronized state, but such conductance increases of single neurons only partly contributed to the observed latency advance. Simultaneous recording from lateral geniculate nucleus (LGN) and V1 neurons using multisite silicon probes revealed that the latency advance increased from LGN to V1 and across successive V1 layers. Thus, the shorter latency of V1 neurons in the desynchronized state can be accounted for by an accumulation of latency advance along various stages in the early visual pathway.

Results

V1 Neurons Respond Faster in Desynchronized Brain State. We used multisite silicon electrodes to record LFP and spiking activity in response to sparse noise stimuli from V1 of head-restrained awake rats (*SI Materials and Methods*). Brain state of awake rats spontaneously alternated between a synchronized state with large-amplitude, slow fluctuations, and a desynchronized state with small-amplitude, fast oscillations (Fig. 1*A*). We analyzed the LFP power in 1–10 and 30–80 Hz for each 2-s segment of the recording and assigned each segment as the synchronized or desynchronized state based on the cluster analysis of LFP power spectrum (Fig. 1*B* and *SI Materials and Methods*). For each neuron, we computed spatiotemporal receptive fields (RFs) using the response epochs in each of the two brain states (*SI Materials and Methods* and Fig. 1*C*). To examine the temporal

Significance

Fast sensory processing, critical for the survival of animals, is usually achieved in a vigilant state characterized by cortical desynchronization. To understand the neural substrate for such fast processing, we examined brain state modulation of response latency in rat primary visual cortex (V1). We found that the response latency for V1 neurons is shorter in the desynchronized state than in the synchronized state. Increase in membrane conductance of single V1 neurons contributes to but cannot fully account for the observed latency advance. Such faster response is explained by cumulative latency advance along various stages of the visual pathway, from lateral geniculate nucleus to successive V1 layers, likely due to a global increase of membrane conductance in the desynchronized state.

Author contributions: X.-d.W., C.C., and H.Y. designed research; X.-d.W., C.C., and D.Z. performed research; X.-d.W., C.C., and D.Z. analyzed data; and X.-d.W., C.C., D.Z., and H.Y. wrote the paper.

The authors declare no conflict of interest.

*This Direct Submission article had a prearranged editor.

[1]X.-d.W. and C.C. contributed equally to this work.

[2]To whom correspondence should be addressed. E-mail: haishanyao@ion.ac.cn.

This article contains supporting information online at www.pnas.org/lookup/suppl/doi:10.1073/pnas.1316166111/-/DCSupplemental.

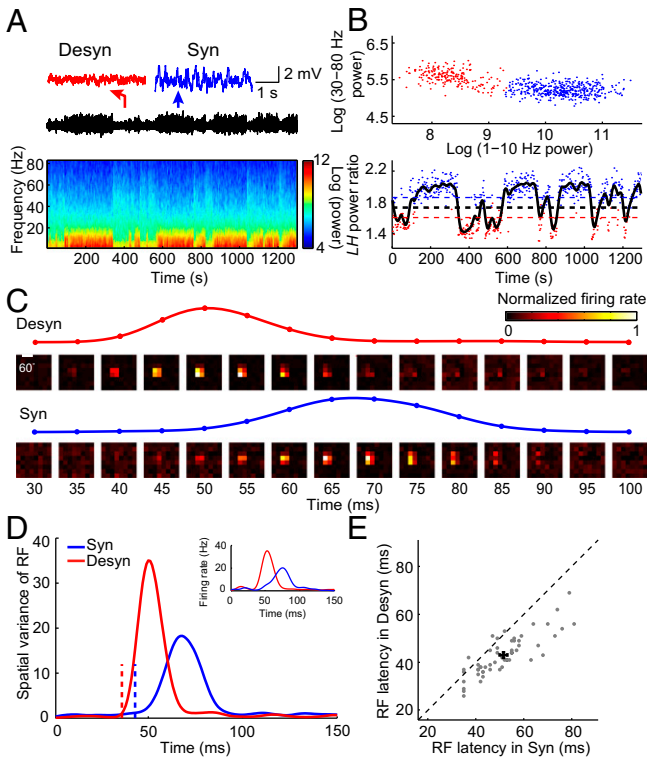

Fig. 1. Latency of spike RF in V1 depends on brain state in awake rats. (*A*) Spontaneous switch of brain states indicated by changes in LFP trace and its power spectrum from a head-fixed awake rat. *Insets* above, magnified LFP traces of 4-s recording from a period in the desynchronized (marked by the red arrow) and the synchronized (marked by the blue arrow) state, respectively. (*B*) (*Upper*) Cluster analysis according to the LFP power in 1–10 and 30–80 Hz (red dots, desynchronized state; blue dots, synchronized state). Each dot was calculated from a 2-s segment of LFP trace shown in *A*. (*Lower*) Classification of synchronized and desynchronized brain states from *LH* power ratio (*SI Materials and Methods*) of the LFP trace. Black curve, smoothed curve of *LH* power ratio of the LFP trace shown in *A*. Blue (red) dots, time segments for the blue (red) clusters in the upper panel. The blue (red) dashed line indicates upper (lower) threshold (*SI Materials and Methods*). The black dashed line, mean of the upper and lower threshold, is the threshold used to separate different brain states. Time segments with *LH* power ratio larger (smaller) than the threshold were defined as synchronized (desynchronized) states. (*C*) Spatiotemporal RF maps of an example V1 neuron shown in a series of time delays after stimulus onset (*Upper*, desynchronized state; *Lower*, synchronized state). The traces above show the time courses of the spatial variance of RF from 30 to 100 ms after stimulus onset. (*D*) Time courses of the spatial variance of RF in desynchronized (red) and synchronized (blue) states for the cell shown in *C*. The dashed lines mark the latencies of RF (desynchronized state: 36 ms; synchronized state: 43 ms). *Inset* shows the spiking responses to the most effective stimulus pixel in the RF (red, desynchronized state; blue, synchronized state). (*E*) Summary of the RF latencies in desynchronized and synchronized states for awake rats ($n = 54$, $P = 1.3 \times 10^{-9}$, Wilcoxon signed rank test). Error bars represent ±SEM.

profile of the RF, we calculated the spatial variance of RF (variance of the responses to different stimulus positions, $\sigma_2 = <[R(x,y) - <R(x,y)>]^2>$; *SI Materials and Methods*) at each time delay after stimulus onset (16, 17) (Fig. 1 *C* and *D*). Response latency was determined from the temporal profile of RF (*SI Materials and Methods*) (18, 19). As shown in Fig. 1 *C* and *D*, the latency of the example cell was shorter in the desynchronized state than in the synchronized state. Over the population, the mean latency measured in the desynchronized state was 43.0 ± 1.2 ms (mean ± SEM), significantly shorter than that (51.6 ± 1.6 ms, mean ± SEM) measured in the synchronized state (Fig. 1*E*, $n = 54$, $P = 1.3 \times 10^{-9}$, Wilcoxon signed rank test).

This brain state modulation of RF latency was also observed for V1 neurons recorded extracellularly from anesthetized rats (Fig. 2). Urethane anesthesia caused spontaneous transitions between different brain states (20) and has been widely used as a model system for studying brain state-dependent sensory processing (11, 21, 22). In this study, we used urethane together with isoflurane (*SI Materials and Methods*) to control brain state in a relatively stable manner (Fig. 2 *A* and *B*). As shown in Fig. 2 *C* and *D*, the example V1 neuron from an anesthetized rat also exhibited latency advance in the desynchronized state. At the population level, the mean latency in the desynchronized state was 48.0 ± 1.3 ms (mean ± SEM), which was 14.4 ± 0.9 ms (mean ± SEM) shorter than that (62.5 ± 1.3 ms, mean ± SEM) in the synchronized state (Fig. 2*E*, $n = 127$, $P = 2.0 \times 10^{-20}$, Wilcoxon signed rank test). Thus, brain state-dependent latency advance was observed in both awake and anesthetized rats.

Shorter Response Latency for Membrane Potential Response of V1 Neurons in Desynchronized State. Besides using extracellular recordings, we further used in vivo whole-cell recordings in anesthetized rats (*SI Materials and Methods*) to examine how brain state modulates the latency of subthreshold membrane potential response (Fig. 3), which results from the integration of excitatory and inhibitory synaptic inputs. Each brain state was

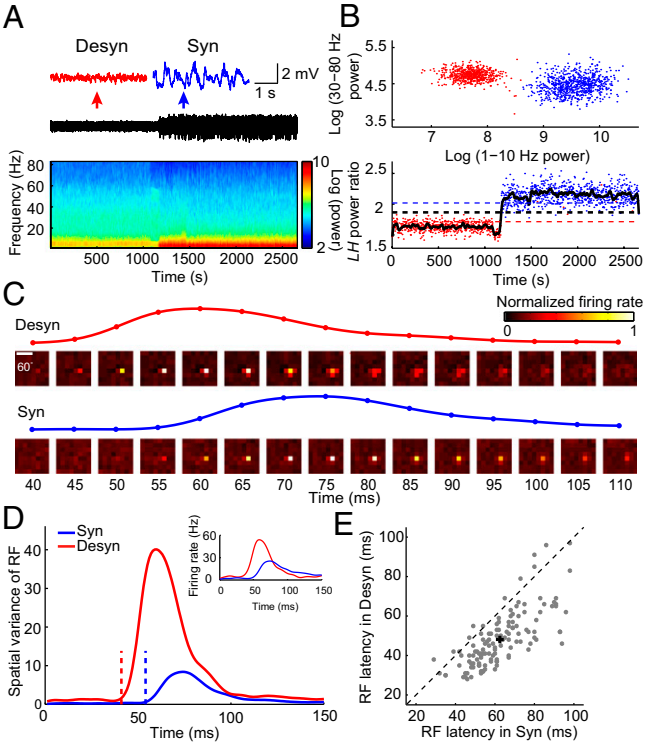

Fig. 2. Latency of spike RF in V1 depends on brain state in anesthetized rats. (*A*) LFP trace and its power spectrum for an anesthetized rat. *Insets* above, magnified LFP traces of 4-s recording for a period in the desynchronized state (marked by the red arrow) and the synchronized state (marked by the blue arrow), respectively. (*B*) Cluster analysis of LFP power, same as described in Fig. 1*B*. (*C*) Spatiotemporal RF maps of an example V1 neuron, same as described in Fig. 1*C*. Traces above show the time courses of the spatial variance of RF from 40 to 110 ms after stimulus onset. (*D*) Time courses of the spatial variance of RF in desynchronized (red) and synchronized (blue) states for the cell shown in *C*. The dashed lines mark the latencies of RF (desynchronized state: 41 ms; synchronized state: 54 ms). *Inset* shows the spiking responses to the most effective stimulus pixel in the RF (red, desynchronized state; blue, synchronized state). (*E*) Summary of the RF latencies in desynchronized and synchronized states for anesthetized rats ($n = 127$, $P = 2.0 \times 10^{-20}$, Wilcoxon signed rank test). Error bars represent ±SEM.

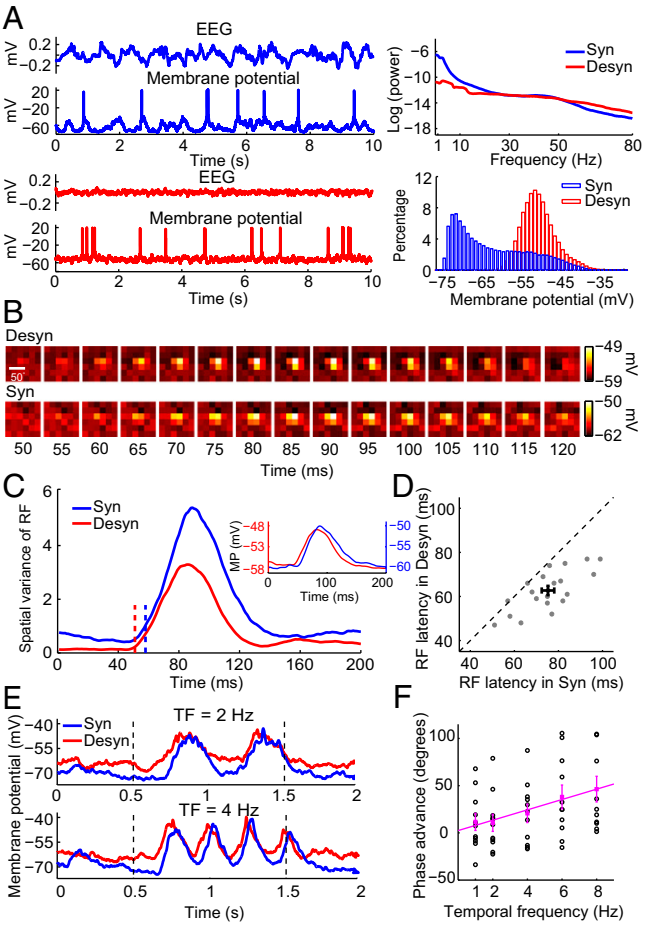

Fig. 3. Brain state-dependent latency advance of membrane potential response of V1 neurons. (*A*) (*Left*) Example EEG and membrane potential (V_m) traces in synchronized (blue) and desynchronized states (red) in anesthetized rats. (*Upper Right*) Power spectrum for EEG in synchronized (blue) and desynchronized (red) states. (*Lower Right*) Distribution of V_m in synchronized (blue) and desynchronized (red) states. (*B*) Spatiotemporal RF maps measured by V_m for an example V1 neuron in desynchronized (*Upper*) and synchronized (*Lower*) states. (*C*) Time courses of spatial variance of subthreshold RF in desynchronized (red) and synchronized (blue) states for the cell shown in *B*. The dashed lines mark the latencies of RF (desynchronized state: 51 ms; synchronized state: 58 ms). *Inset* shows the subthreshold membrane potential responses (MP) to the most effective stimulus pixel in the RF (red, desynchronized state; blue, synchronized state). (*D*) Summary of the RF latencies for V_m response in desynchronized and synchronized states ($n = 20$, $P = 1.5 \times 10^{-4}$, Wilcoxon signed rank test). Error bars represent ±SEM (*E*) Example V_m responses to drifting gratings at different temporal frequencies (*Upper*, 2 Hz; *Lower*, 4 Hz) in synchronized (blue) and desynchronized (red) states. The dashed lines denote onset and offset of drifting grating. (*F*) Phase advance, the difference between the phase of F1 component of V_m in the desynchronized state and that in the synchronized state, is plotted against temporal frequency ($n = 11$). Each black circle represents the phase advance of each neuron; the filled magenta square is the mean phase advance. Error bars represent ±SEM. Magenta line, linear regression between the mean phase advance and temporal frequency ($R^2 = 0.96$, $P = 0.0035$, *F* test). The slope of the line determines the latency advance, which is 15.2 ms (95% confidence interval: 9.5–21.0 ms).

characterized by a distinct pattern of EEG and membrane potential that were simultaneously recorded (Fig. 3*A*). The EEG recorded in the desynchronized state exhibited less low-frequency power and more high-frequency power than that in the synchronized state. Membrane potential usually showed a unimodal distribution in the desynchronized state, but a bimodal distribution in the synchronized state. Similar to the RF measured by spiking activities, RF measured by membrane potentials exhibited shorter latency in the desynchronized state than in the synchronized state (Fig. 3 *B–D*, $n = 20$, latency advance was 12.6 ± 2.0 ms, mean ± SEM; $P = 1.5 \times 10^{-4}$, Wilcoxon signed rank test). In addition to measuring latency from the responses to sparse noise, we also measured latency from the responses to drifting gratings of different temporal frequencies (*SI Materials and Methods*). As shown by the example cell in Fig. 3*E*, the membrane potential responses in the desynchronized state were phase-advanced relative to those in the synchronized state. The brain state-dependent phase advance here is reminiscent of the contrast-dependent phase advance, i.e., the response latency of V1 neurons shortens as the contrast of visual stimuli increases (23, 24). Thus, by analogy to the contrast-dependent phase advance, the brain state-dependent phase advance was defined as the difference between the phase of first harmonic (F1 component) of membrane potential response in the desynchronized state and that in the synchronized state. The latency advance, as computed from the slope of linear regression between the brain state-dependent phase advance and temporal frequency (*SI Materials and Methods*), was 15.2 ms (95% confidence interval: 9.5–21.0 ms; Fig. 3*F*; $n = 11$, $R^2 = 0.96$, $P = 0.0035$, *F* test), comparable to that measured from the temporal profile of RF (Figs. 2*E* and 3*D*).

Membrane Conductance of V1 Neurons Increases in Desynchronized State. Different brain states are associated with different network activities, which play important roles in modifying the temporal properties of synaptic integration by cortical neurons (14, 15). Thus, we raised a hypothesis that brain state modulates response latency of V1 neurons by changing background synaptic inputs. To test this hypothesis, we calculated the resting conductances from the same cells undergoing the two brain states by recording membrane currents (potentials) at multiple holding voltages (currents) (25–28) (*SI Materials and Methods*). We found the resting conductance in the desynchronized state was higher than that in the synchronized state (Fig. 4). We also calculated the visually evoked conductances in the two states. As shown in Fig. 4*A*, for the responses to both 4- and 8-Hz drifting gratings, the peak amplitudes of the evoked excitatory (ΔG_e), inhibitory (ΔG_i), and total conductances ($G_{tot} = G_{rest} + \Delta G_e + \Delta G_i$) of the example cell were higher in the desynchronized state than in the synchronized state. Such conductance increases in the desynchronized state were observed over the population (Fig. 4*B*; $n = 7$, G_{rest}, $P = 0.016$; ΔG_e, $P = 0.047$; ΔG_i, $P = 0.016$; G_{tot}, $P = 0.016$; Wilcoxon signed rank test), with a nearly 100% increase in total conductance.

The higher resting membrane conductance in the desynchronized state can be attributed to stronger background synaptic bombardments, which elevate the resting membrane potential. In addition, the larger total conductance (including both the resting and visually evoked conductances) in the desynchronized state leads to a smaller membrane time constant. We estimated the contribution of such conductance increases to the latency advance in a single-neuron model (*SI Materials and Methods*), in which the neuron receives stronger background and visually evoked synaptic inputs in the desynchronized state, based on our experimental results. In this model, stronger background inputs produce a more depolarized resting membrane potential (Fig. S1*A*), consistent with our experimental results and previous reports (15, 29). We found that the latency advance estimated from such conductance increases was 4.4 ms (95% confidence interval: 3.0–5.7 ms; Fig. S1*B*; $n = 20$, $R^2 = 0.97$, $P = 0.002$, *F* test), which only constituted a small fraction of the measured latency advance (Fig. 3*F*). This indicates that the conductance increase of a single V1 neuron alone is not sufficient to account for the latency advance measured experimentally.

Latency Advance Accumulates from LGN to V1 and Across Successive V1 Layers. As transition between brain states involves a global change of network dynamics, conductance increase in the

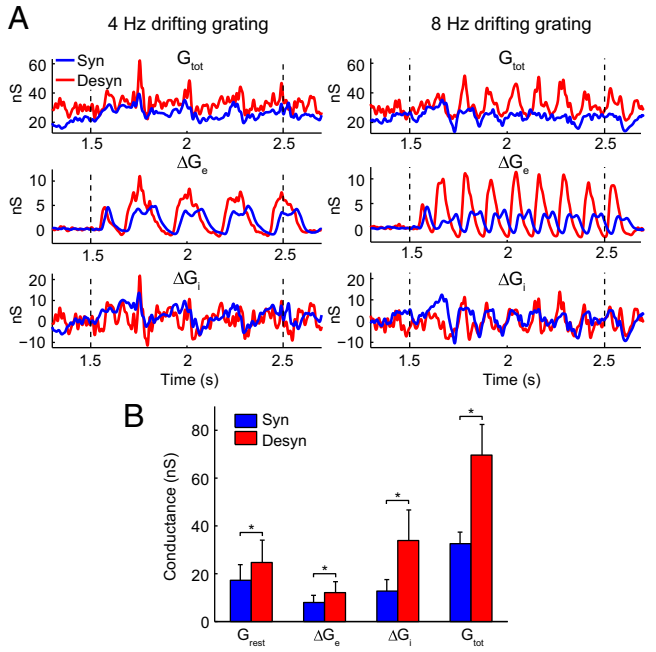

Fig. 4. Comparison of membrane conductance for V1 neurons between two brain states. (*A*) Conductance of an example neuron in synchronized (blue) and desynchronized (red) states measured with 4-Hz gratings (left column) and 8-Hz gratings (right column). The dashed lines denote onset and offset of drifting grating. Top row, total membrane conductance (G_{tot}). G_{rest} was calculated from the spontaneous activity before the onset of drifting grating. Middle row, evoked excitatory synaptic conductance (ΔG_e). Bottom row, evoked inhibitory synaptic conductance (ΔG_i). (*B*) Increase of conductance in the desynchronized state ($n = 7$). The evoked conductances were measured by the magnitudes of peak conductances. For cells measured with both 4- and 8-Hz gratings, we averaged the magnitudes measured under the two gratings. Error bars represent SEM. *$P < 0.05$, Wilcoxon signed rank test.

desynchronized state is likely to be a global effect. We thus further hypothesized that latency advance exists at various stages of the visual pathway, and V1 neurons inherit part of their latency advance from LGN neurons. To test this hypothesis, we first examined the response latency of LGN neurons, which were simultaneously recorded with V1 neurons using two 16-site silicon electrodes in anesthetized rats (*SI Materials and Methods*). As shown by the LFP traces in Fig. 5*A*, the transition between the two brain states occurred simultaneously in the two brain regions. Fig. 5*B* shows the temporal profiles of RFs for an example pair of simultaneously recorded LGN and V1 cells under the two brain states. Similar to V1 neurons, LGN neurons also exhibited latency advance (Fig. 5*C*; $n = 98$, $P = 1.6 \times 10^{-10}$, Wilcoxon signed rank test), but with a degree (10.4 ± 1.6 ms, mean ± SEM) significantly smaller than that for V1 neurons (14.4 ± 0.9 ms, mean ± SEM) (Fig. 5*D*; $n = 127$ for V1 and $n = 98$ for LGN, $P = 0.0067$, Wilcoxon rank sum test), indicating that the latency advance accumulates from LGN to V1. Thus, the latency advance in V1 can be attributed to that of LGN and that contributed by the conductance increase of V1 neurons.

To examine whether the latency advance also accumulates along successive stages of information processing across V1 layers, we next measured LFP responses in the two brain states to full-screen flash for all 16 recording sites located at different cortical depths. We performed current source density (CSD) analysis to transform the LFP responses into current sources and sinks (Fig. 6*A*), which are local synaptic activities that generate LFP, and provide more precise spatial information than LFP about the location of cortical layer (30, 31). Layer 4 was defined as the location exhibiting the earliest response of current sinks, layer 2/3 was defined as those sites located above layer 4, and layer 5 was those sites located immediately below layer 4 and exhibited latency longer than that in layer 4 (32) (Fig. 6*B*). By estimating response latency from the CSD profiles at each layer (*SI Materials and Methods* and Fig. 6*B*), we found that the absolute latency increased sequentially from layer 4 to layer 2/3 and layer 5 in both brain states (Fig. 6*C*; $n = 7$; synchronized state: $P = 0.016$ for layer 4 versus layer 2/3 and for layer 2/3 versus layer 5; desynchronized state: $P = 0.031$ for layer 4 versus layer 2/3; $P = 0.016$ for layer 2/3 versus layer 5; Wilcoxon signed rank test), consistent with the sequence of cortical information flow (32). Interestingly, the latency advance grew from layer 4 to layer 2/3 to layer 5 (Fig. 6*D*; $n = 7$; layer 4 versus layer 2/3: $P = 0.031$; layer 2/3 and layer 5: $P = 0.047$; Wilcoxon signed rank test). Taken together, these results support our hypothesis that latency advance accumulates at various stages of the visual pathway, from LGN to successive V1 layers, likely due to a global increase of membrane conductance in the desynchronized state (Fig. 6*E*).

Discussion

Our study showed that V1 neurons responded faster in the desynchronized brain state than in the synchronized brain state. Both the resting and the evoked conductances of V1 neurons increased in the desynchronized state. Such conductance increases of single V1 neurons shorten the response latency by elevating the membrane potential closer to the firing threshold and reducing the membrane time constant, but the effects only account for a small fraction of the observed latency advance. The latency advance of V1 neurons can be explained by a cumulative effect: latency advance of LGN neurons contributed to that of V1 neurons, and latency advance in V1 accumulated from layer 4 to layer 2/3 to layer 5, likely due to the global conductance increase associated with the brain state change. Such cumulative latency advance may also apply to visual areas beyond V1 (Fig. 6*E*) and play a particularly important role for fast neural processing in higher visual areas.

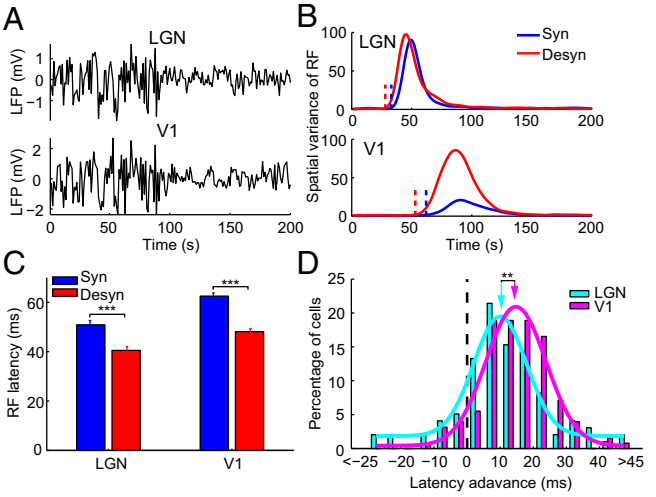

Fig. 5. Comparison of latency advance between LGN and V1 neurons. (*A*) Simultaneously recorded LFP traces in LGN and V1. (*B*) Time courses of spatial variance of RF for an example pair of simultaneously recorded LGN and V1 neurons in synchronized (blue) and desynchronized (red) states. The vertical dashed lines denote latencies of the RFs. (*C*) RF latency for a population of LGN and V1 neurons in synchronized (blue) and desynchronized (red) states (LGN, $n = 98$; V1, $n = 127$). Error bars represent SEM. ***$P < 0.001$, Wilcoxon signed rank test. (*D*) Distribution of latency advance for LGN (cyan) and V1 (magenta) neurons. The arrows point to the mean latency advance (10.4 ms for LGN; 14.4 ms for V1). **$P < 0.01$, Wilcoxon rank sum test.

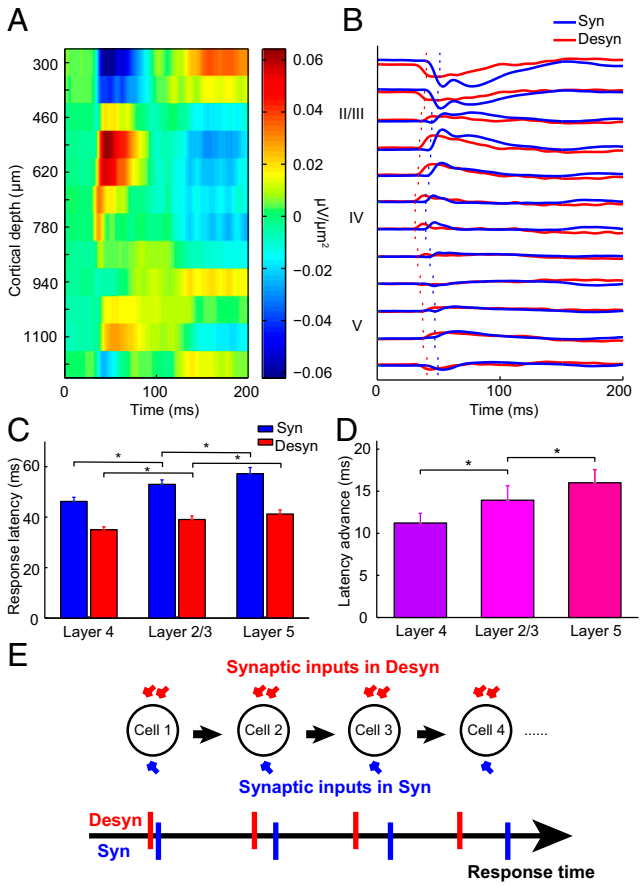

Fig. 6. CSD responses indicate cumulative latency advance across successive V1 layers. (*A*) An example CSD map derived from LFPs measured across V1 layers. (*B*) CSD traces across layers in synchronized (blue) and desynchronized (red) states. The dashed lines indicate the onset latencies. (*C*) Population summary of response latency of CSD for layer 4, layer 2/3, and layer 5 in synchronized (blue) and desynchronized (red) states ($n = 7$). Error bars represent SEM. $^*P < 0.05$, Wilcoxon signed rank test. (*D*) Latency advance increased across V1 layers ($n = 7$). Error bars represent SEM. $^*P < 0.05$, Wilcoxon signed rank test. (*E*) A schematic showing cumulative latency advance along the visual pathway.

Conductance Increase in Desynchronized State. Our result on the increase of resting membrane conductance in the desynchronized state is consistent with a previous study, which showed that the input resistance of neurons in the barrel cortex is smaller in the active whiskering period (similar to the desynchronized state) than in the quiet awakefulness (similar to the synchronized state) (33). A recent study compared conductances of V1 neurons between awake (mainly in the desynchronized state) and anesthetized (in the synchronized state) mice (34). Consistent with their results, we also found that inhibitory conductance dominated in the desynchronized state (Fig. 4*B*). However, the latter study reported no changes of resting and total conductances. This discrepancy may be due to the fact that we compared conductances measured from the same neuron undergoing the two states, whereas the latter study compared conductances of different neurons from two animal groups.

Shifts between brain states can be mediated by neuromodulatory systems, whose overall effect on the cortex is to put it in an activated state during cortical desynchronization (4, 5). Intense background synaptic bombardments in the desynchronized state can lead to an increase in the resting conductance of V1 neurons. The increase of visually evoked conductance in the desynchronized state in V1 may result from stronger synaptic inputs from LGN neurons, because the evoked responses of LGN neurons are significantly enhanced in the desynchronized state (Fig. S2*A*), consistent with previous studies (10, 12).

Potential Mechanism for Brain State-Dependent Latency Advance of LGN Neurons. When the brain state changes from the synchronized to the desynchronized state, LGN neuronal response shifts from burst to tonic mode, with membrane potential closer to the firing threshold (35, 36). In addition, we found that both the spontaneous and evoked firing rates of LGN neurons increased in the desynchronized state (Fig. S2), likely leading to higher resting and total conductances. Similar to V1 neurons, the elevated membrane potential and shortened membrane time constant caused by the conductance increase can both contribute to the latency advance of LGN neurons. Furthermore, retinal ganglion cell responses in rat can be modulated by brain state, possibly mediated by the serotonin input to the retina from the dorsal raphe (37). Therefore, retinal ganglion cells may also exhibit brain state-dependent latency advance, which can contribute to that of LGN neurons.

Cumulative Effect of Latency Advance. The brain state-dependent latency advance reported here is reminiscent of the phase advance of V1 neurons caused by high-contrast visual stimuli (23, 24). To account for the contrast-dependent phase advance, the resistor–capacitor implementation of the normalization model (38, 39) proposes that high-contrast stimulus increases the conductance of the V1 neuron by enhancing the activities of other V1 neurons connecting to it. The conductance increase results in the reduction of membrane time constant, leading to phase advance. This mechanism of conductance increase successfully explains a variety of contrast-dependent nonlinear responses of V1 neurons, but the membrane conductance of V1 neurons has to become very large to account for the contrast-dependent phase advance (39). Our study showed that conductance increase of single V1 neurons accounts for a small fraction of the measured latency advance, and the latency advance of a V1 neuron is due to a cumulative effect, which incorporates the latency advance inherited from its input neurons and that contributed by its own conductance increase. By analogy to our finding, one study reported that the contrast-induced phase advance was larger in V1 than in LGN (40). Thus, the cumulative effect revealed here may be applied to the contrast-dependent latency advance along the visual pathway. In addition to the contrast-dependent latency advance, contrast-gain control can also accumulate across multiple processing stages (41, 42). Thus, cumulative effect may be a general implementation for efficient processing of visual information.

Brain State Modulation of Response Latency in Various Sensory Modalities. A previous study in barrel cortex of awake mice found no significant difference of response latency between the quiet and actively whisking periods (33). The response latency reported in the latter study was less than 10 ms, much smaller than that in V1, due to only three synaptic relays from sensory receptors to the barrel cortex (43). The small number of synaptic relays before sensory information reaching the barrel cortex may limit the cumulative effect. In addition, we found that the distinction between the desynchronized and synchronized states in awake animals was not as prominent as that in anesthetized animals (*SI Materials and Methods* and Fig. S3 *A* and *B*), and latency advance was indeed smaller in awake than in anesthetized animals (Figs. 1*E* and 2*E*). Therefore, the effect of brain state on response latency in the barrel cortex may be too small to be detectable. Another study in the primary auditory cortex of marmosets also found no difference in response latency between slow-wave sleep and awake state (44). Because the awake state includes both synchronized and desynchronized states, identification of state-dependent response latency in the auditory cortex may require further studies that more precisely define the brain state. Consistent with our results, a recent study in mouse V1 also showed shorter latency of subthreshold response in awake

(mainly in the desynchronized state) than in anesthetized (mainly in the synchronized state) animals (figure S3 in ref. 34). Notably, the response latency of V1 neurons depended on the degree of cortical synchronization rather than whether the animal is awake or anesthetized (Fig. S3). The latency in the desynchronized state of anesthetized rats was shorter than that in the synchronized state but longer than that in the desynchronized state of awake rats (Fig. S3*D*), indicating the importance of identifying brain states for both anesthetized and awake animals.

Desynchronized State and Selective Attention. Interestingly, there are many similarities between the desynchronized state and the pattern of cortical activity associated with selective attention (4). It is suggested that common neuromodulatory systems are involved in regulating attention and cortical desynchronization (4, 5), and attention may lead to a reduction in response latency (45). Indeed, attention-induced latency advance has been observed in monkey V4 (46, 47) and MT (48), and the shorter latency of visual response correlates with faster reaction of the animal (47, 48). Because selective attention may involve local desynchronization of neuronal activity along the visual pathway representing the attended stimulus (4, 49), the cumulative effect revealed here may play a role in visual processing during selective attention. It is of interest for future study to investigate whether attention also leads to cumulative latency advance along various stages of visual processing. Furthermore, because rapid reaction of vigilant animals is likely due to fast processing of both sensory input and motor output, the cumulative effect revealed in this study may be also important for the motor system and lead to fast motor processing.

Materials and Methods

All experiments were approved by the Animal Care and Use Committee at the Institute of Neuroscience, Chinese Academy of Sciences. Data analyses and single-neuron model were implemented using MATLAB. For details of rat preparation, recordings, visual stimulation, data analysis, and modeling, see *SI Materials and Methods*.

ACKNOWLEDGMENTS. We thank W.-Q. Xu and H.-Y. Zhong for technical assistance and M.-H. Long for help with the awake recordings. We thank M.-M. Poo, M. Carandini, and K. Harris for critical reading of and comments on the manuscript. This work was supported by 973 Program Grant 2011CBA00401.

1. Raz A, Buhle J (2006) Typologies of attentional networks. *Nat Rev Neurosci* 7(5): 367–379.
2. Eason RG, Harter MR, White C (1969) Effects of attention and arousal on visually evoked cortical potentials and reaction time in man. *Physiol Behav* 4(3):283–289.
3. Buck L (1966) Reaction time as a measure of perceptual vigilance. *Psychol Bull* 65(5): 291–304.
4. Harris KD, Thiele A (2011) Cortical state and attention. *Nat Rev Neurosci* 12(9): 509–523.
5. Lee SH, Dan Y (2012) Neuromodulation of brain states. *Neuron* 76(1):209–222.
6. Steriade M (2001) Impact of network activities on neuronal properties in corticothalamic systems. *J Neurophysiol* 86(1):1–39.
7. Steriade M, Timofeev I, Grenier F (2001) Natural waking and sleep states: A view from inside neocortical neurons. *J Neurophysiol* 85(5):1969–1985.
8. Gilbert CD, Sigman M (2007) Brain states: Top-down influences in sensory processing. *Neuron* 54(5):677–696.
9. Haider B, McCormick DA (2009) Rapid neocortical dynamics: Cellular and network mechanisms. *Neuron* 62(2):171–189.
10. Livingstone MS, Hubel DH (1981) Effects of sleep and arousal on the processing of visual information in the cat. *Nature* 291(5816):554–561.
11. Wörgötter F, et al. (1998) State-dependent receptive-field restructuring in the visual cortex. *Nature* 396(6707):165–168.
12. Bezdudnaya T, et al. (2006) Thalamic burst mode and inattention in the awake LGNd. *Neuron* 49(3):421–432.
13. Niell CM, Stryker MP (2010) Modulation of visual responses by behavioral state in mouse visual cortex. *Neuron* 65(4):472–479.
14. Destexhe A, Paré D (1999) Impact of network activity on the integrative properties of neocortical pyramidal neurons in vivo. *J Neurophysiol* 81(4):1531–1547.
15. Destexhe A, Rudolph M, Paré D (2003) The high-conductance state of neocortical neurons in vivo. *Nat Rev Neurosci* 4(9):739–751.
16. Yeh CI, Xing D, Williams PE, Shapley RM (2009) Stimulus ensemble and cortical layer determine V1 spatial receptive fields. *Proc Natl Acad Sci USA* 106(34):14652–14657.
17. Malone BJ, Kumar VR, Ringach DL (2007) Dynamics of receptive field size in primary visual cortex. *J Neurophysiol* 97(1):407–414.
18. Bredfeldt CE, Ringach DL (2002) Dynamics of spatial frequency tuning in macaque V1. *J Neurosci* 22(5):1976–1984.
19. Mazer JA, Vinje WE, McDermott J, Schiller PH, Gallant JL (2002) Spatial frequency and orientation tuning dynamics in area V1. *Proc Natl Acad Sci USA* 99(3):1645–1650.
20. Clement EA, et al. (2008) Cyclic and sleep-like spontaneous alternations of brain state under urethane anaesthesia. *PLoS One* 3(4):e2004.
21. Curto C, Sakata S, Marguet S, Itskov V, Harris KD (2009) A simple model of cortical dynamics explains variability and state dependence of sensory responses in urethane-anesthetized auditory cortex. *J Neurosci* 29(34):10600–10612.
22. Murakami M, Kashiwadani H, Kirino Y, Mori K (2005) State-dependent sensory gating in olfactory cortex. *Neuron* 46(2):285–296.
23. Albrecht DG (1995) Visual cortex neurons in monkey and cat: Effect of contrast on the spatial and temporal phase transfer functions. *Vis Neurosci* 12(6):1191–1210.
24. Dean AF, Tolhurst DJ (1986) Factors influencing the temporal phase of response to bar and grating stimuli for simple cells in the cat striate cortex. *Exp Brain Res* 62(1): 143–151.
25. Anderson JS, Carandini M, Ferster D (2000) Orientation tuning of input conductance, excitation, and inhibition in cat primary visual cortex. *J Neurophysiol* 84(2):909–926.
26. Borg-Graham LJ, Monier C, Frégnac Y (1998) Visual input evokes transient and strong shunting inhibition in visual cortical neurons. *Nature* 393(6683):369–373.
27. Monier C, Fournier J, Frégnac Y (2008) In vitro and in vivo measures of evoked excitatory and inhibitory conductance dynamics in sensory cortices. *J Neurosci Methods* 169(2):323–365.
28. Priebe NJ, Ferster D (2005) Direction selectivity of excitation and inhibition in simple cells of the cat primary visual cortex. *Neuron* 45(1):133–145.
29. Destexhe A, Rudolph M, Fellous JM, Sejnowski TJ (2001) Fluctuating synaptic conductances recreate in vivo-like activity in neocortical neurons. *Neuroscience* 107(1): 13–24.
30. Mitzdorf U (1985) Current source-density method and application in cat cerebral cortex: Investigation of evoked potentials and EEG phenomena. *Physiol Rev* 65(1): 37–100.
31. Nicholson C, Freeman JA (1975) Theory of current source-density analysis and determination of conductivity tensor for anuran cerebellum. *J Neurophysiol* 38(2): 356–368.
32. Douglas RJ, Martin KA (2004) Neuronal circuits of the neocortex. *Annu Rev Neurosci* 27:419–451.
33. Crochet S, Petersen CC (2006) Correlating whisker behavior with membrane potential in barrel cortex of awake mice. *Nat Neurosci* 9(5):608–610.
34. Haider B, Häusser M, Carandini M (2013) Inhibition dominates sensory responses in the awake cortex. *Nature* 493(7430):97–100.
35. McCormick DA (1992) Neurotransmitter actions in the thalamus and cerebral cortex and their role in neuromodulation of thalamocortical activity. *Prog Neurobiol* 39(4): 337–388.
36. Sherman SM, Guillery RW (2002) The role of the thalamus in the flow of information to the cortex. *Philos Trans R Soc Lond B Biol Sci* 357(1428):1695–1708.
37. Galambos R, Szabó-Salfay O, Szatmári E, Szilágyi N, Juhász G (2001) Sleep modifies retinal ganglion cell responses in the normal rat. *Proc Natl Acad Sci USA* 98(4): 2083–2088.
38. Carandini M, Heeger DJ (1994) Summation and division by neurons in primate visual cortex. *Science* 264(5163):1333–1336.
39. Carandini M, Heeger DJ, Movshon JA (1997) Linearity and normalization in simple cells of the macaque primary visual cortex. *J Neurosci* 17(21):8621–8644.
40. Alitto HJ, Usrey WM (2004) Influence of contrast on orientation and temporal frequency tuning in ferret primary visual cortex. *J Neurophysiol* 91(6):2797–2808.
41. Carandini M, Heeger DJ (2012) Normalization as a canonical neural computation. *Nat Rev Neurosci* 13(1):51–62.
42. Sit YF, Chen Y, Geisler WS, Miikkulainen R, Seidemann E (2009) Complex dynamics of V1 population responses explained by a simple gain-control model. *Neuron* 64(6): 943–956.
43. Petersen CC (2007) The functional organization of the barrel cortex. *Neuron* 56(2): 339–355.
44. Issa EB, Wang X (2011) Altered neural responses to sounds in primate primary auditory cortex during slow-wave sleep. *J Neurosci* 31(8):2965–2973.
45. Reynolds JH, Heeger DJ (2009) The normalization model of attention. *Neuron* 61(2): 168–185.
46. Sundberg KA, Mitchell JF, Gawne TJ, Reynolds JH (2012) Attention influences single unit and local field potential response latencies in visual cortical area V4. *J Neurosci* 32(45):16040–16050.
47. Womelsdorf T, Fries P, Mitra PP, Desimone R (2006) Gamma-band synchronization in visual cortex predicts speed of change detection. *Nature* 439(7077):733–736.
48. Galashan FO, Saßen HC, Kreiter AK, Wegener D (2013) Monkey area MT latencies to speed changes depend on attention and correlate with behavioral reaction times. *Neuron* 78(4):740–750.
49. Kastner S, Pinsk MA (2004) Visual attention as a multilevel selection process. *Cogn Affect Behav Neurosci* 4(4):483–500.